INFLUENCE OF STRAIN HARDENING ON THE BEHAVIOUR AND DESIGN OF STEEL STRUCTURES

LEROY GARDNER[1]

[1] *Imperial College London, Department of Civil Engineering,*
South Kensington Campus, London.
SW7 2AZ, UK
Leroy.gardner@imperial.ac.uk

FACHENG WANG[2]

[2] *Imperial College London, Department of Civil Engineering,*
South Kensington Campus, London.
SW7 2AZ, UK
F.wang07@imperial.ac.uk

ANDREW LIEW[3]

[3] *Imperial College London, Department of Civil Engineering,*
South Kensington Campus, London.
SW7 2AZ, UK
a.liew10@imperial.ac.uk

Received (Day Month Year)
Accepted (Day Month Year)

Abstract

The present generation of international structural steel design codes treat material nonlinearity through simplified elastic-plastic or rigid-plastic material models. However, the actual stress-strain response of structural steel is more complex than this and features, in particular, strain hardening. Strain hardening refers to the increase in strength beyond yield as a result of plastic deformation. The influence of strain hardening on the behaviour and design of steel structures is examined in this study both through experimentation and the analysis of existing data, and a method to exploit the additional capacity that arises is outlined. Both determinate and indeterminate structures are considered. The proposed design method, referred to as the Continuous Strength Method (CSM), is a deformation based design approach employing a continuous relationship between cross-section slenderness and cross-section deformation capacity, together with a material model that allows for strain hardening. Comparisons are made between test results generated as part of the present study and collected from existing studies, and the predictions from the CSM and Eurocode 3 (EC3). For all cases considered, the Continuous Strength Method, through a rational exploitation of strain hardening, offers a more accurate prediction of observed physical behaviour.

Keywords: Bending; Continuous Strength Method; Continuous beams; Deformation capacity; Indeterminate structures; Plastic design; Portal frames; Steel structures; Strain hardening.

Notation

A	Cross-sectional area
b	Section width
COV	Coefficient of variation
CSM	Continuous Strength Method
DSM	Direct Strength Method
E	Young's modulus
E_{sh}	Strain hardening modulus
f_{cr}	Elastic buckling stress
f_{csm}	CSM limiting stress
f_y	Material yield strength
F_{coll}	Plastic collapse load
F_{csm}	Collapse load predicted by CSM
F_{EC3}	Collapse load predicted by EC3
F_u	Test collapse load
h	Section depth
h_i	Section depth at hinge i
h_w	Web height between flanges
L	Length
M_{el}	Elastic moment capacity
M_{pl}	Plastic moment capacity
M_i	Moment at hinge i
M_{csm}	Bending resistance predicted by the CSM
M_{EC3}	Bending resistance predicted by EC3
M_u	Ultimate test moment capacity
N	Axial load
N_{coll}	Plastic collapse load
N_{csm}	Compression resistance
N_{EC3}	Compression resistance
N_u	Ultimate test load
N_y	Yield load
r_i	Internal corner radius
RHS	Rectangular hollow section
SHS	Square hollow section
t	Thickness
t_f	Flange thickness
t_w	Web thickness
v	Vertical beam displacement
v_{max}	Maximum vertical beam displacement
W_{el}	Elastic section modulus
W_{pl}	Plastic section modulus
x	Distance along beam
α	Hinge demand at hinge i
α_{max}	Hinge demand at critical hinge
δ	End shortening/virtual displacement

δ_u End shortening at ultimate load
ε_{csm} CSM limiting strain
ε_{lb} Local buckling strain
ε_y Yield strain
λ_p Plate slenderness
θ Rotation
θ_{pl} Elastic rotation at M_{pl}
θ_i Rotation at hinge i
θ_{max} Rotation at critical hinge

1. Introduction

Strain hardening refers to the increase in strength of metallic materials beyond yield as a result of plastic deformation. This increase in strength is not systematically utilised in current international steel design codes, though allowance is made for the spread of plasticity throughout cross-sections (i.e. use of the plastic moment capacity) and redistribution of moments within an indeterminate structural frame until a collapse mechanism forms (i.e. plastic design). Both of these design techniques are synonymous with simplified elastic-plastic and rigid-plastic material modelling. This limits the resistance of cross-sections in compression to the yield load N_y (defined as the cross-sectional area A, multiplied by the material yield strength f_y) and the resistance of cross-sections in bending to the plastic moment capacity M_{pl} (defined as the plastic section modulus W_{pl} multiplied by f_y).

The influence of strain hardening on the load carrying capacity of structural steel elements is investigated in the present study through laboratory testing and analysis of existing structural performance data from the literature. Consideration is first given to the behaviour of determinate structures, such as simple beams and columns, before proceeding to study the response of indeterminate structures, including continuous beams and frames. A new design approach, the Continuous Strength Method (CSM), has been developed that offers a systematic means of utilising strain hardening, based on cross-section deformation capacity.[1] The method allows the attainment of compression resistances greater than the yield load as well as bending resistances beyond the plastic moment capacity, resulting in better prediction of observed structural behaviour. In this paper, a brief account of the experimental study is reported, development and extension of the Continuous Strength Method is described and comparisons with test results and current design practice are made.

2. Experimental Study

2.1. Introduction

An experimental programme comprising tensile coupon tests, measurements of geometric imperfections and residual stresses, 20 stub column tests, 6 simple beam tests and 12 continuous beam tests has been carried out at Imperial College London, to investigate the structural behaviour of determinate and indeterminate structures. Both hot-rolled (S355)

and cold-formed (S235) hollow sections have been examined and the tested specimens were generally of stocky proportions in order to suppress premature local buckling and assess the influence of stain hardening. A summary of the experiments performed and the key results obtained is presented herein, while a more detailed account of the testing programme is reported in Ref. 2.

2.2. Material and stub column tests

Tensile coupon tests on material extracted from the flat regions of each of the examined cross-sections were performed to determine the basic engineering stress-strain characteristics of the material. The obtained yield strengths (taken as the 0.2% proof strengths for cold-formed material) are presented in Table 1, and have been used in the analysis of the member test results. Full details of the coupon tests have been reported in Ref. 2. A total of 20 stub column tests were carried out, two repeated tests on each section size denoted 1 and 2 in Table 1.

Table 1. Geometric properties and ultimate load carrying capacities of the stub columns

Stub column specimen	L mm	h mm	b mm	t mm	r_i mm	A mm^2	f_y N/mm^2	N_u kN
SHS 100×100×4-HR1	405.2	100.01	100.89	4.09	2.75	1543	488	706
SHS 100×100×4-HR2	405.2	99.83	100.84	4.11	2.75	1548	488	707
SHS 100×100×4-CF1	405.0	100.55	100.56	3.59	6.38	1342	482	660
SHS 100×100×4-CF2	404.8	100.75	100.68	3.61	6.13	1353	482	663
SHS 60×60×3-HR1	245.0	60.21	60.18	3.35	2.38	739	449	353
SHS 60×60×3-HR2	245.1	60.22	60.23	3.38	2.44	745	449	363
SHS 60×60×3-CF1	245.1	60.30	60.14	2.78	3.75	614	361	249
SHS 60×60×3-CF2	245.1	60.17	60.17	2.79	3.88	615	361	250
RHS 60×40×4-HR1	245.0	59.84	40.09	3.83	1.88	682	468	344
RHS 60×40×4-HR2	244.9	59.72	40.17	3.83	1.94	681	468	346
RHS 60×40×4-CF1	244.9	60.09	40.07	3.95	2.19	701	400	370
RHS 60×40×4-CF2	244.9	60.06	40.00	3.97	1.94	705	400	370
SHS 40×40×4-HR1	165.2	40.00	39.94	3.91	2.06	537	496	333
SHS 40×40×4-HR2	165.1	40.05	39.94	3.91	2.25	536	496	335
SHS 40×40×4-CF1	165.1	40.36	40.32	3.76	3.13	518	410	256
SHS 40×40×4-CF2	165.2	40.32	40.31	3.79	3.06	522	410	256
SHS 40×40×3-HR1	165.0	40.25	40.23	3.05	2.13	435	504	263
SHS 40×40×3-HR2	165.2	40.16	40.10	3.05	2.00	434	504	257
SHS 40×40×3-CF1	165.2	40.12	40.13	2.76	2.56	394	451	224
SHS 40×40×3-CF2	165.1	40.04	40.07	2.75	2.69	391	451	230

The specimen designation begins with the section size, e.g. SHS 100×100×4, followed by the production route - HR for hot-rolled and CR for cold-formed, and finally the test number - 1 or 2. The geometric properties and ultimate load carrying capacities are also

reported in Table 1, in which L is the specimen length, b and h are the outer cross-section width and depth dimensions, t is the section thickness, r_i is the internal corner radius, A is the cross-sectional area and N_u is the ultimate test load.

Typical normalised load-end shortening responses for both hot-rolled and cold-formed sections (SHS 40×40×3-HR1 and SHS 40×40×3-CF1) are shown in Fig. 1. On the vertical axis, the axial load N has been normalised by the yield load Af_y and on the horizontal axis, the end shortening δ of the test specimens has been normalised by the stub column length L. The influence of strain hardening, characterised by load-carrying capacities in excess of the yield load (i.e. the Eurocode resistance for stocky sections), may be seen for both the hot-rolled and cold-formed sections. The hot-rolled sections exhibit a yield plateau before the commencement of strain hardening, while the cold-formed sections display a more rounded response. For the cold-formed sections, part of the additional capacity beyond the yield load may be attributed to the enhanced strength in the corner regions of the sections, arising from high localised plastic deformations during production. Corner strength enhancements were measured as part of the experimental programme through tensile testing of corner coupons. For the cold-formed SHS shown in Fig. 1, the yield strength of the corner material was 534 N/mm^2, resulting in an increased yield load of the section (based on weighted average calculations) of 6%.

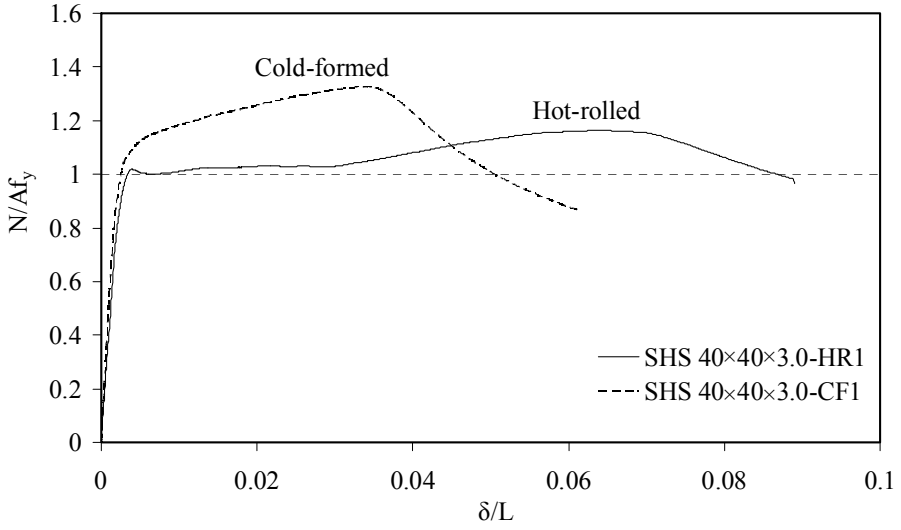

Fig. 1. Typical normalised load-end shortening graphs from stub column tests

The results obtained from the stub column tests reported above have been combined with those from previous studies and analysed in Section 3 of this paper.

2.3. Simple beam tests

A total of 6 simply supported beam tests were conducted in three-point bending to obtain the basic flexural response characteristics and ultimate moment capacities of hot-rolled

and cold-formed sections. Full details of the tests are reported in Ref. 2, while a summary of the tests is presented in Table 2, in which W_{pl} is the plastic section modulus, M_{pl} is the plastic moment capacity $W_{pl}f_y$ and M_u is the ultimate test moment capacity. Note that all of the test specimens are Class 1 or 2 according to Eurocode 3. Typical normalised moment-rotation curves for hot-rolled and cold-formed sections RHS 60×40×4-HR and RHS 60×40×4-CF are shown in Fig. 2. On the vertical axis, the moment M has been normalised by the plastic moment capacity M_{pl}, and on the horizontal axis, the central rotation θ (calculated as the sum of the end rotations) has been normalised by the elastic rotation at the plastic moment θ_{pl}.

Table 2. Summary of simple beam tests

Simple beam specimen	h mm	b mm	t mm	r_i mm	W_{pl} mm^3	M_{pl} kNm	M_u kNm
SHS 40×40×4-HR	39.75	40.00	3.91	2.16	7080	3.51	3.84
SHS 40×40×4-CF	40.31	40.42	3.70	3.10	6900	2.83	3.61
SHS 40×40×3-HR	39.87	40.20	3.05	2.07	5900	2.97	3.44
SHS 40×40×3-CF	40.16	40.11	2.80	2.63	5500	2.48	3.09
RHS 60×40×4-HR	60.09	40.24	3.90	1.91	13400	6.27	7.14
RHS 60×40×4-CF	60.04	40.09	3.93	2.07	13400	5.37	7.59

Similar strain hardening characteristics to those seen in the stub column tests may be observed, with ultimate test moments in excess of the plastic moment capacity. The results from the beam tests are analysed in Section 3, in conjunction with data obtained from existing test programmes.

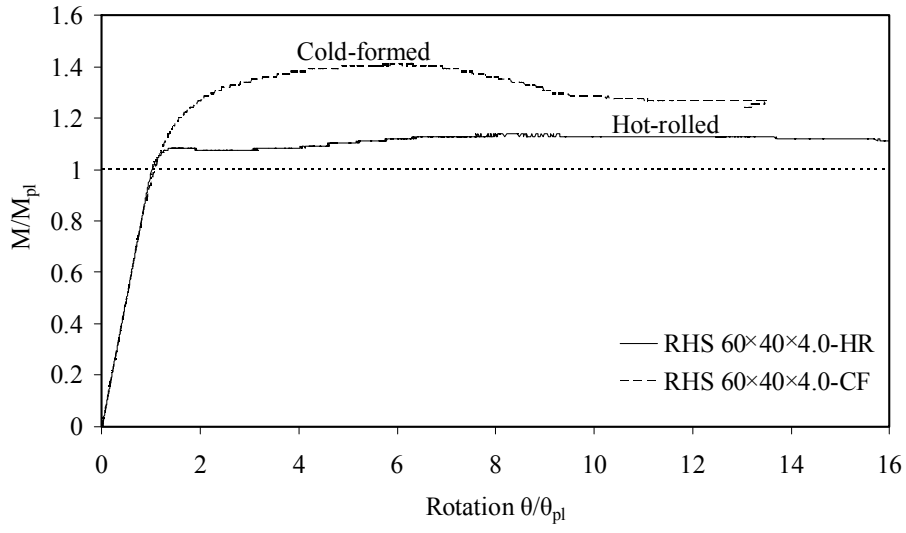

Fig. 2. Typical normalised moment-rotation curves from simple beam tests

2.4. Continuous beam tests

A total of 12 two-span continuous beam tests were carried out to investigate the structural response and strain hardening characteristics of indeterminate steel structures. The same 6 nominal section sizes as tested in the simply supported setup were analysed. Tests were conducted in two configurations, as indicated by the final number in the specimen designation - in configuration 1, equal point loads were applied centrally in the two spans (denoted 1/2 span in Table 3), while in configuration 2, equal point loads were applied at a third of each span length from the central support (denoted 1/3 span in Table 3). The two different loading positions were employed to vary the load level between the formation of the first plastic hinge and the final collapse mechanism, which also creates differing rotation demands on the first plastic hinge. The test specimen geometries and key results are summarised in Table 3, where F_u refers to the value of total load at collapse (i.e. the sum of the two point loads). Further details of the continuous beam tests are reported in Ref. 2.

Table 3. Summary of two-span continuous beam tests

Continuous beam specimen	Configuration	h mm	b mm	t mm	r_i mm	W_{pl} mm^3	F_u kN
RHS 60×40×4-HR1	1/2 span	60.09	40.27	3.85	1.91	13300	78.1
SHS 40×40×4-HR1	1/2 span	39.79	39.98	3.85	2.16	7010	44.6
SHS 40×40×3-HR1	1/2 span	39.90	40.22	3.01	2.07	5850	38.1
RHS 60×40×4-CF1a	1/2 span	60.14	40.20	3.89	2.07	13400	83.4
RHS 60×40×4-CF1b	1/2 span	60.15	40.08	3.87	2.07	13300	83.3
SHS 40×40×4-CF1	1/2 span	40.37	40.36	3.72	3.10	6930	40.6
SHS 40×40×3-CF1	1/2 span	40.08	40.20	2.72	2.63	5370	34.2
RHS 60×40×4-HR2	1/3 span	60.06	40.33	3.82	1.91	13200	98.4
SHS 40×40×4-HR2	1/3 span	39.93	39.78	3.90	2.16	7090	55.2
SHS 40×40×3-HR2	1/3 span	40.21	39.91	3.02	2.07	5890	49.0
SHS 40×40×4-CF2	1/3 span	40.43	40.36	3.71	3.10	6930	51.6
SHS 40×40×3-CF2	1/3 span	40.12	40.14	2.76	2.63	5430	42.3

Typical normalised load-end rotation graphs for hot-rolled and cold-formed specimens RHS 60×40×4-HR1 and RHS 60×40×4-CF1a are shown in Fig. 3 for the 1/2 span loading configuration. On the vertical axis, the test load F has been normalised by the calculated plastic collapse load F_{coll} for the continuous beam, and on the horizontal axis is the end rotation θ (in radians). For the continuous beams, strain hardening may be seen to result in collapse loads greater than those predicted by traditional plastic methods. More detailed analysis of the results of the continuous beam tests and comparisons with different design approaches are presented in Section 3 of this paper.

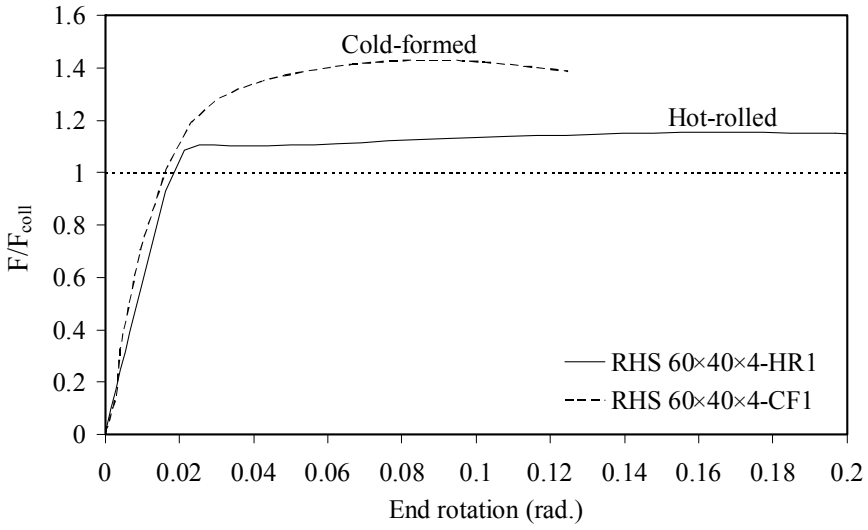

Fig. 3. Normalised load-end rotation curves from continuous beam tests

3. The Continuous Strength Method (CSM)

3.1. Introduction

The influence of strain hardening on the capacity of structural steel members has been illustrated through the experiments presented in Section 2 of this paper. The results have shown that the limiting resistances adopted in present design practice of the yield load in compression for stub columns, the plastic moment capacity in bending for determinate structures and the plastic collapse load for indeterminate structures are conservative in the case of stocky sections. The ability of a cross-section to sustain increased loading and indeed deform into the strain hardening regime, is limited by the effects of local buckling. Susceptibility to local buckling is currently assessed by means of cross-section classification, where structural cross-sections are assigned to discrete behavioural classes depending on the slenderness of the constituent elements. The Continuous Strength Method[1] is an alternative approach to calculating cross-section resistance, which is based on a continuous relationship between cross-section slenderness and deformation capacity and a rational exploitation of strain hardening. Development of the method for both determinate and indeterminate structures is described below.

3.2. CSM for determinate structures

The CSM recognises that the resistance of structural cross-sections is a continuous function of their deformation capacity, as controlled by the slenderness (and hence propensity to local buckling) of the constituent plate elements. The method employs a continuous base curve (Fig. 4), defining the relationship between cross-section slenderness and cross-section deformation capacity, together with a material model that allows for the influence of strain hardening (Fig. 5). The CSM currently applies only to fully effective (i.e. non-slender) sections, though extension of the method to allow for partial plastification of slender sections is under consideration. Determination of cross-section capacities in compression and bending, incorporating recent developments to the method is summarised in the following sub-sections.

3.2.1 Cross-section compression resistance

Within the Continuous Strength Method, cross-section slenderness is defined through Eq. (3.1) by the plate slenderness of the most slender constituent element in the section:

$$\overline{\lambda}_p = \sqrt{f_y / f_{cr}} \tag{3.1}$$

where f_y is the material yield strength and f_{cr} is the elastic buckling stress, taking due account of the element support conditions and the applied stress distribution as set out in EN 1993-1-5[3]. Alternatively, as in the Direct Strength Method (DSM)[4], the slenderness of the full cross-section rather than that of the most slender constituent element may be employed. This approach has been found to offer modest improvements in the accuracy of the method for the sections considered herein (I sections, SHS and RHS); the benefits are more significant in the case of slender sections with more complex geometries where element interaction and the influence on the elastic buckling behaviour is more pronounced. Having established the cross-section slenderness, the corresponding normalised deformation capacity of the cross-section $\varepsilon_{csm}/\varepsilon_y$, referred to as the strain ratio, is then obtained through the base curve given by Eq. (3.2) and shown in Fig. 4.

$$\frac{\varepsilon_{csm}}{\varepsilon_y} = \frac{0.4}{\overline{\lambda}_p^{\,3.2}} \quad \text{but} \quad \frac{\varepsilon_{csm}}{\varepsilon_y} \le 15 \quad \text{for} \quad \overline{\lambda}_p \le 0.748 \tag{3.2}$$

in which $\varepsilon_y = f_y / E$ is the yield strain of the material, E is the Young's modulus, and ε_{csm} is the CSM limiting strain of the section. The base curve Eq. (3.2) was generated as described in Ref. 1 by means of stub column test data, including those described herein together with further data collected from previous studies[5-10]. In interpreting the test data, for stocky sections, where the ultimate load N_u is greater than the yield load N_y, the CSM limiting strain ε_{csm} is based on the local buckling strain $\varepsilon_{lb} = \delta_u / L$, defined as the end shortening at ultimate load δ_u normalised by the stub column length L.

For materials that exhibit a well defined yield stress, such as hot-rolled sections, the strain ratio $\varepsilon_{csm}/\varepsilon_y$ is given by Eqn. (3.3).

$$\frac{\varepsilon_{csm}}{\varepsilon_y} = \frac{\varepsilon_{lb}}{\varepsilon_y} \qquad N_u \ge N_y \tag{3.3}$$

For materials that exhibit a more rounded, non-linear stress-strain response, such as with cold-formed sections, the strain ratio involves the subtraction of the plastic strain at the 0.2% proof stress (i.e. 0.2%) as in Eq. (3.4).

$$\frac{\varepsilon_{csm}}{\varepsilon_y} = \frac{\varepsilon_{lb} - 0.002}{\varepsilon_y} \qquad N_u \ge N_y \tag{3.4}$$

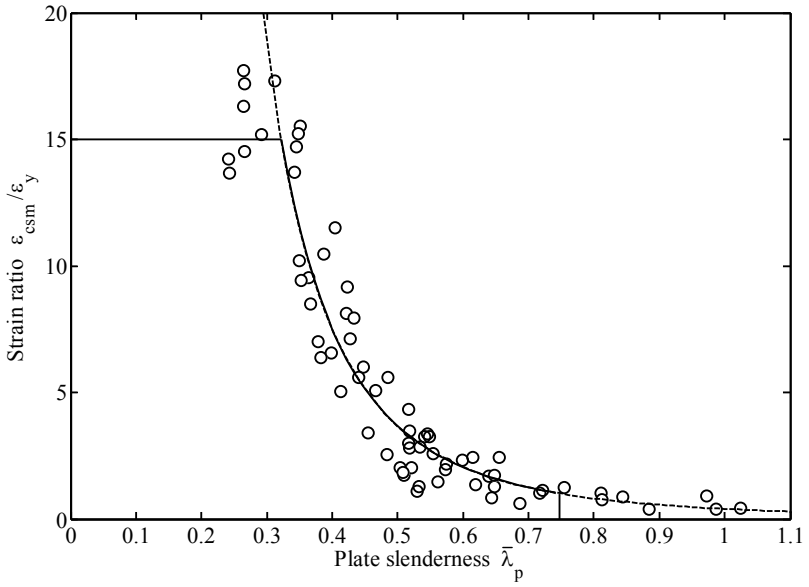

Fig. 4. Base curve – relationship between strain ratio and slenderness

For slender sections ($N_u < N_y$), where the response is influenced by elastic post-buckling behaviour, the strain ratio $\varepsilon_{csm}/\varepsilon_y$ is defined as the ratio of the ultimate load N_u to the yield load N_y as given by Eq. (3.5).

$$\frac{\varepsilon_{csm}}{\varepsilon_y} = \frac{N_u}{N_y} \qquad N_u < N_y \tag{3.5}$$

Since slender sections fail below their yield load, where stress is proportional to strain, adoption of Eq. (3.5) yields a normalised relationship between deformation capacity and slenderness that is similar to that between strength and slenderness given by the familiar Winter curve. Following recent developments, the base curve defined by Eq. (3.2) now differs from that presented previously[1] due to: (1) Availability and inclusion of further test data[2,5,7-10] upon which to establish the curve; (2) Element slenderness is defined using flat plate widths, in line with EN 1993-1-1[11], rather than centreline dimensions; (3) Applicability of the method has been limited to sections with slenderness no greater than 0.748, with more slender sections being covered by the existing effective width[3] or Direct Strength Methods; (4) A limit of 15 has been placed on the strain ratio, which corresponds to the material ductility requirement expressed in EN 1993-1-1[11]; (5) Plotting of test data points accounts for element interaction by using the slenderness of the complete section, calculated by means of Ref. 12, rather than that of the most slender element. Having established the strain ratio of the section, the CSM limiting stress f_{csm} is determined directly from the strain hardening material model shown in Fig. 5 which shows the adopted bi-linear, elastic-linear hardening material model, with strain hardening slope $E_{sh}=E/100$ as recommended in EN 1993-1-5[3].

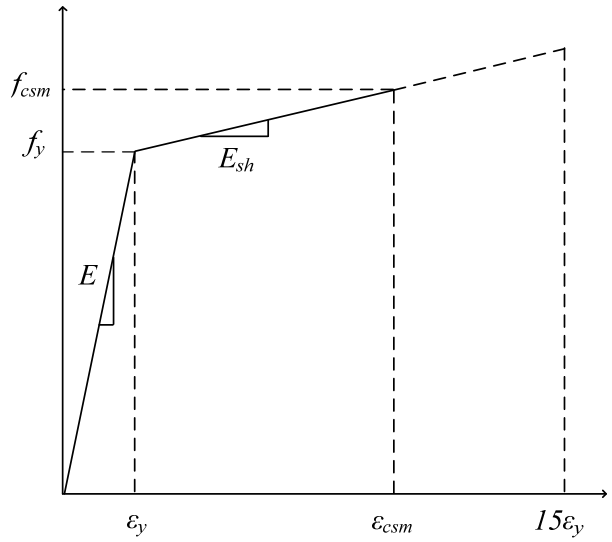

Fig. 5. Bi-linear stress-strain material model

Finally, the cross-section compression resistance N_{csm} is given by Eq. (3.6) as the product of the gross cross-section area A and the limiting stress f_{csm}.

$$N_{csm} = Af_{csm} \tag{3.6}$$

where f_{csm} is determined from the strain hardening material model given by Eq. (3.7):

$$f_{csm} = f_y + E_{sh}\left(\varepsilon_{csm} - \varepsilon_y\right) \qquad \varepsilon_{csm} \geq \varepsilon_y \tag{3.7}$$

While a strain hardening modulus E_{sh} of E/100 has been adopted for all section types in the current study, this value has been found to be conservative for cold-formed sections, partly due to the influence of the enhanced strength at corner regions, and a value of E/50 may be acceptable. Further investigation is underway in this area.

3.2.2. Cross-section bending resistance

Assuming plane sections remain plane and normal to the neutral axis in bending, the corresponding linear strain and bi-linear stress distributions for one half of a symmetric section is shown in Fig. 6, this represents the major axis with a cross-section depth of h. A cross-section where the strain ratio $\varepsilon_{csm}/\varepsilon_y \geq 1$ implies the limiting stress f_{csm} is equal to or has exceeded the yield stress f_y , hence the cross-section has met or exceeded its elastic moment capacity M_{el}.

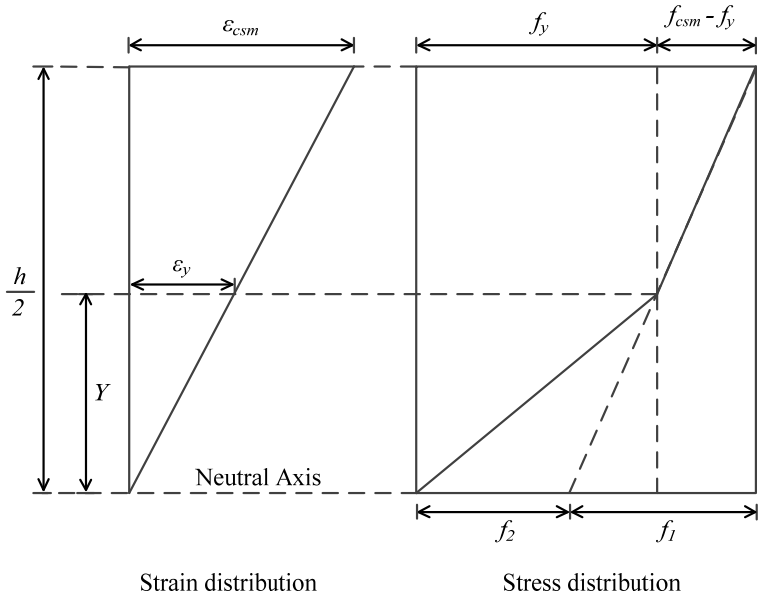

Fig. 6. Stress distribution geometry from linear strain assumption for $\varepsilon_{csm}/\varepsilon_y \geq 1$

From Fig. 6, a general expression for moment capacity M_{csm}, in terms of the elastic section modulus W_{el}, plastic section modulus W_{pl} and an additional modulus W_w, is given by:

$$M_{csm} = W_{pl} f_{csm} - (W_{pl} - W_{el}) f_1 - W_w f_2 \tag{3.8}$$

With the distance from the neutral axis to the point of first yield as $Y=0.5h(\varepsilon_{csm}/\varepsilon_y)^{-1}$ and the expression for the limiting stress f_{csm} established from Eq. (3.7), stresses f_1 and f_2 are:

$$\frac{f_1}{f_y} = \frac{E_{sh}}{E}\frac{\varepsilon_{csm}}{\varepsilon_y} \qquad \frac{f_2}{f_y} = 1 - \frac{E_{sh}}{E} \tag{3.9}$$

Substituting f_1 and f_2 into Eq. (3.8) and normalising by M_{pl} gives:

$$\frac{M_{csm}}{M_{pl}} = 1 + \frac{E_{sh}}{E}\left(\frac{\varepsilon_{csm}}{\varepsilon_y}\frac{W_{el}}{W_{pl}} - 1\right) - \frac{W_w}{W_{pl}}\left(1 - \frac{E_{sh}}{E}\right) \tag{3.10}$$

The term $W_w f_2$ in Eq. (3.8), represents the moment M_{f2} associated with the triangular shaped stress block linked with stress f_2 for $y \le Y$ (see Fig. 6).

$$M_{f_2} = W_w f_2 = \int f y dA_Y = \int f_2 g(y) y dA_Y, \quad \text{hence}$$

$$W_w = \int g(y) y dA_Y \tag{3.11}$$

The integral is only evaluated up to $y=Y$, hence the associated area is termed A_Y; the function $g(y)$ represents the stress distribution normalised to f_2. As the stress distribution and section geometry is relatively simple, discretising into rectangles and triangles is suitable. For box and I sections bending about the y-y axis, Y will generally lie within the web of practical sections, giving:

$$W_w = \frac{t_w h^2}{12}\left(\frac{\varepsilon_{csm}}{\varepsilon_y}\right)^{-2} \qquad \text{for} \qquad \frac{\varepsilon_{csm}}{\varepsilon_y} \ge 1 + \frac{2t_f}{h_w} \tag{3.12}$$

For low strain ratios, Y may enter the flanges leading to:

$$W_w = \frac{bh^2}{12}\left(\frac{\varepsilon_{csm}}{\varepsilon_y}\right)^{-2} - \frac{(b-t_w)}{12} h_w^2 \left(3 - \frac{2h_w}{h}\right)\frac{\varepsilon_{csm}}{\varepsilon_y}$$

$$\text{for} \qquad 1 \le \frac{\varepsilon_{csm}}{\varepsilon_y} < 1 + \frac{2t_f}{h_w} \tag{3.13}$$

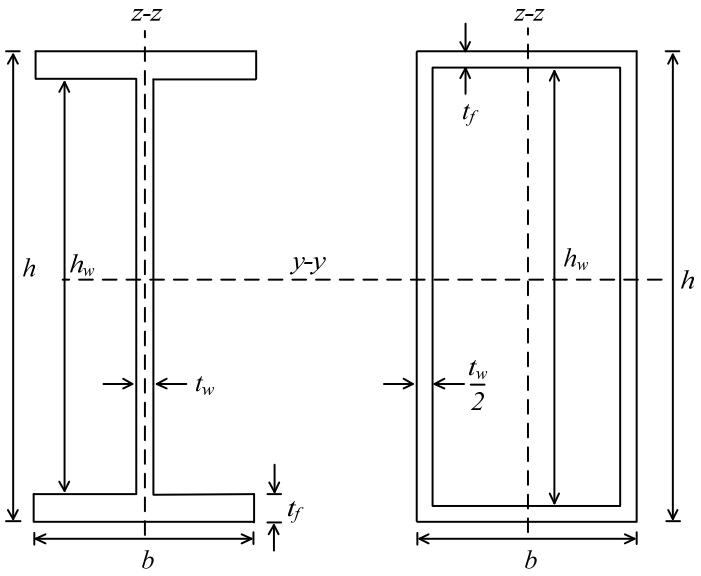

Fig. 7. Section geometry

The section geometry used for the derivation of W_w is defined in Fig. 7. Note that the equivalent web thickness t_w for box sections is twice the wall thickness. Analytic expressions have also been developed for circular hollow sections, and I/box sections bending about the minor axis. The generated expressions are exact, but are rather lengthy for practical design due in particular, to the W_w term.

By inspection it can be seen from Fig. 6, that when $\varepsilon_{csm}/\varepsilon_y=1$, the triangular stress block for f_2 overlaps with that of f_1, hence $W_w=W_{pl}-W_{el}$. Inserting this into Eq. (3.10) at a strain ratio of 1 shows that the overall expression collapses on the right hand side to M_{el}/M_{pl}. From Eq. (3.12) and Eq. (3.13), the decay of W_w, with respect to strain ratio can be shown to be conservatively taken as:

$$W_w = (W_{pl} - W_{el})\left(\frac{\varepsilon_{csm}}{\varepsilon_y}\right)^{-2} \tag{3.14}$$

Combining with Eq. (3.10), the general moment equation can be expressed with only three ratios, the ratio of strain hardening modulus to Young's modulus E_{sh}/E, W_{el}/W_{pl} and the strain ratio $\varepsilon_{csm}/\varepsilon_y$, as given by Eq. (3.15):

$$\frac{M_{csm}}{M_{pl}} = 1 + \frac{E_{sh}}{E}\left(\frac{\varepsilon_{csm}}{\varepsilon_y}\frac{W_{el}}{W_{pl}} - 1\right) - \left(1 - \frac{W_{el}}{W_{pl}}\right)\left(1 - \frac{E_{sh}}{E}\right)\left(\frac{\varepsilon_{csm}}{\varepsilon_y}\right)^{-2} \tag{3.15}$$

By noting that in general $E_{sh}/E<<1$, the $(1-E_{sh}/E)$ term can be conservatively (as the final term is subtractive) taken as 1, and the rest of the equation forced through M_{el} at $\varepsilon_{csm}/\varepsilon_y=1$ by Eq. (3.16).

$$\frac{M_{csm}}{M_{pl}} = 1 + \frac{E_{sh}}{E}\frac{W_{el}}{W_{pl}}\left(\frac{\varepsilon_{csm}}{\varepsilon_y} - 1\right) - \left(1 - \frac{W_{el}}{W_{pl}}\right)\left(\frac{\varepsilon_{csm}}{\varepsilon_y}\right)^{-2} \tag{3.16}$$

Fig. 8 shows, for a typical I section beam, the normalised moment prediction M/M_{pl} versus strain ratio for the design expression Eq. (3.16), the exact analytical equation Eq. (3.10) and a previous model proposed by Kemp et al[13], that also allows capacities beyond M_{pl} due to strain hardening. The simple design expression may be seen to closely follow the exact solution, tending towards it for increasing strain ratio where W_w is less influential.

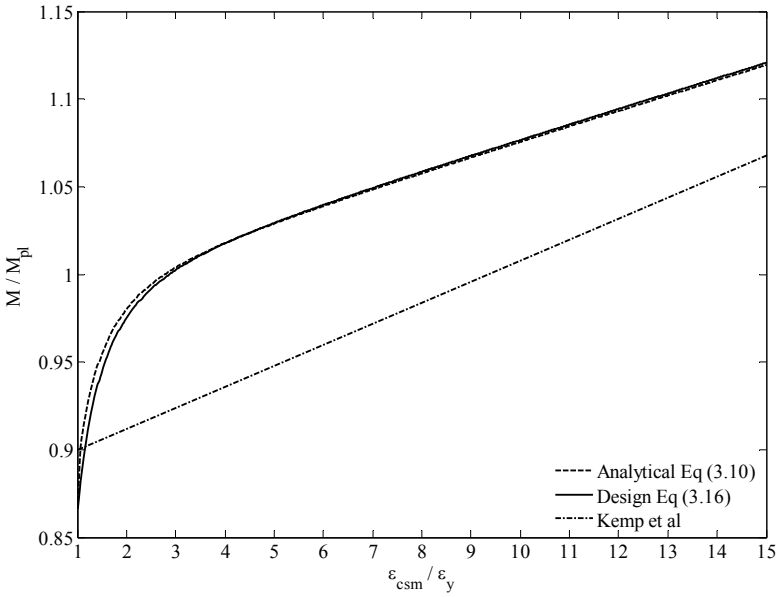

Fig. 8. Analytical, design and Kemp et al relationships between normalised moment capacity and strain ratio

3.2.3. Comparisons between test data and design models

Comparison of the CSM predictions with the results of stub column and simple beam tests are shown in Fig. 9 and Fig. 10 respectively, in which the Eurocode design model is also depicted. The presented test data (comprising cruciforms, I sections and square and rectangular hollow sections) were obtained from Refs 2,5-10,14 and 15. In Fig. 10, the CSM design expression Eq. (3.16) is displayed for E_{sh}/E=1/100 and a shape factor of 1.25 which is representative of the data set. The maximum strain ratio of $\varepsilon_{csm}/\varepsilon_y=15$, gives a cap to M_u/M_{pl} for slenderness values below 0.322.

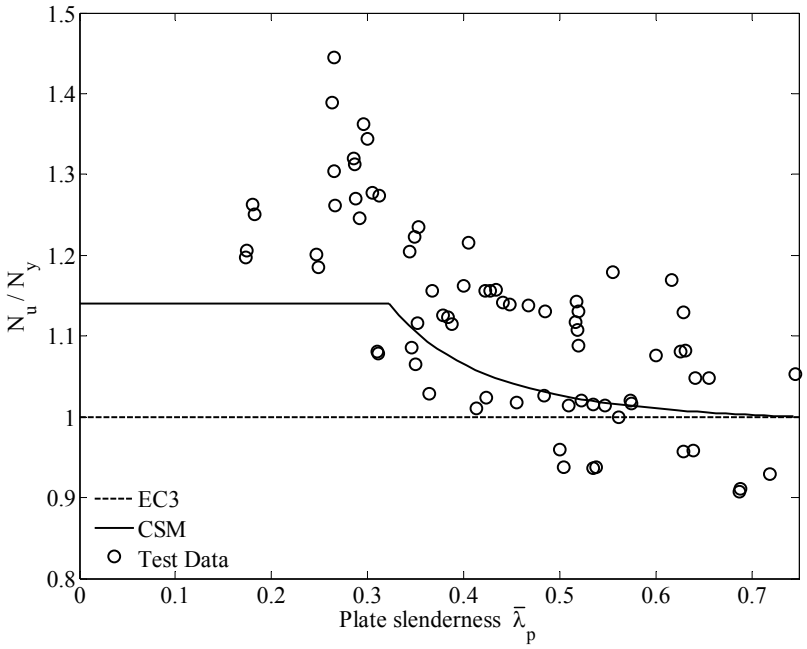

Fig. 9. Stub column test data and comparison with design models

Numerical comparisons, including the mean and coefficient of variation (COV), of the CSM and Eurocode predictions with test data are presented in Tables 4 and 5. The results show that the CSM offers more accurate prediction of the test data and a reduction in scatter.

Table 4. Comparison of the CSM and Eurocode methods with stub column test results

No. of tests: 74	N_{EC3} / N_u	N_{csm} / N_u	N_{csm} / N_{EC3}
Mean	0.889	0.947	1.07
COV	0.108	0.078	-

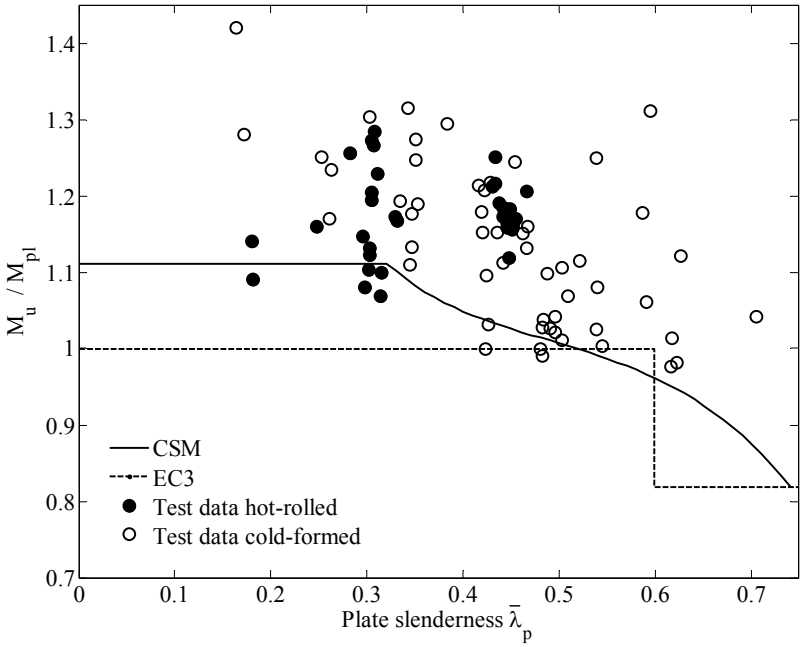

Fig. 10. Simple beam test data and comparison with design models

Table 5. Comparison of the CSM and Eurocode methods with bending test results

No. of tests: 88	M_{EC3} / M_u	M_{csm} / M_u	M_{csm} / M_{EC3}
Mean	0. 865	0. 915	1.06
COV	0.076	0.069	-

3.3. CSM for indeterminate structures

3.3.1 Introduction

Indeterminate steel structures are generally designed using traditional plastic analysis methods, which are based on the formation and subsequent rotation of plastic hinges at their full plastic moment capacity. The formation of each plastic hinge causes a progressive reduction in stiffness of the structure until the final hinge forms resulting in a collapse mechanism. In reality though, plastic hinges do not rotate at a constant moment equal to M_{pl} due to the occurrence of strain hardening, with stockier sections often achieving resistances significantly beyond those predicted by current design approaches. The importance of strain hardening in indeterminate structures has been described by Ref. 16, which observed that enhanced capacity could be attained in steel frames by considering strain hardening provided local and lateral-torsional buckling were eliminated.

3.3.2 Design approach

A new design approach that combines features of the traditional plastic design method and the CSM has been developed to determine the collapse loads of indeterminate steel structures, with due allowance for the influence of strain hardening. For a given collapse mechanism, the critical plastic hinge is first identified as the one that undergoes the greatest deformation demand relative to the deformation capacity of the cross-section at that location. The demands at other plastic hinge locations are then assigned relative to that of the critical hinge. In cases of constant section sizes, the critical hinge is simply the one that undergoes maximum rotation. Based on the resulting demands, the corresponding bending moment diagram at collapse is determined. For plastic design the strain ratio at any hinge *i* should satisfy Eq. (3.17).

$$\left(\frac{\varepsilon_{csm}}{\varepsilon_y} \right)_i \geq \frac{\varepsilon_p}{\varepsilon_y} \tag{3.17}$$

where $\varepsilon_p / \varepsilon_y$ is the plastic strain ratio, which represents the strain ratio when $M_{csm} / M_{pl} = 1$ from Eq. (3.16). For typical sections this can be taken as 3.0 for I sections and 3.6 for box sections bending about their major axis. Thus a hinge is defined as a cross-section that has reached M_{pl} and rotates at a reduced flexural stiffness of $E_{sh} I$ until M_{csm} is reached.

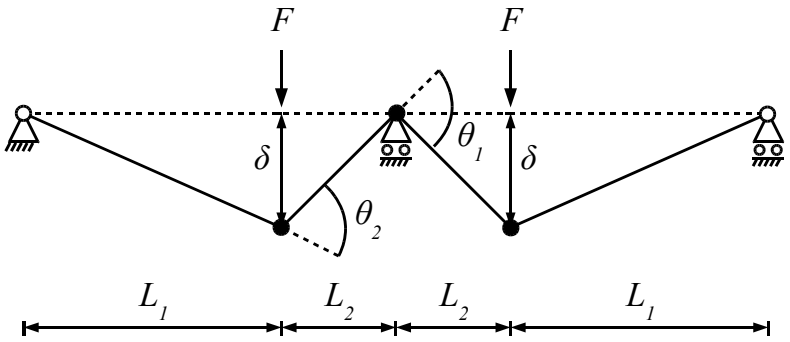

Fig. 11. Plastic collapse mechanism for two-span continuous beam

The key design steps, applied for illustration purposes to the two-span continuous beam shown in Fig. 11, where θ_1 and θ_2 are plastic hinge rotations and δ is a virtual displacement, are summarised as followed:

(1) Identify the locations of the plastic hinges in a manner similar to traditional plastic design and determine the hinge rotations θ_i.

(2) Based on each hinge rotation θ_i, section height h_i and strain ratio $(\varepsilon_{csm}/\varepsilon_y)_i$ calculate the corresponding hinge demands α_i from Eq. (3.18).

$$\alpha_i = \frac{\theta_i h_i}{\left(\frac{\varepsilon_{csm}}{\varepsilon_y}\right)_i} \tag{3.18}$$

The critical hinge is identified as the one with the highest hinge demand $\alpha_{max}=max\{\alpha_i\}$, with the strain ratio at this hinge now labelled $(\varepsilon_{csm}/\varepsilon_y)_{\max}$.

(3) Calculate the corresponding bending moments M_i at the plastic hinges from Eq. (3.16) using $(\varepsilon_{csm}/\varepsilon_y)_{hinge,i}$ as defined in Eq. (3.19).

$$\left(\frac{\varepsilon_{csm}}{\varepsilon_y}\right)_{hinge,i} = \frac{\alpha_i}{\alpha_{\max}}\left(\frac{\varepsilon_{csm}}{\varepsilon_y}\right)_{\max} \quad \text{but} \quad \left(\frac{\varepsilon_{csm}}{\varepsilon_y}\right)_{hinge,i} \le \left(\frac{\varepsilon_{csm}}{\varepsilon_y}\right)_i \tag{3.19}$$

(4) Produce the collapse bending moment diagram as shown in Fig. 12. Note that in this case the two hinges forming in the spans undergo the same rotation θ_2, giving equal moments M_2, the internal support rotation and moment being θ_1 and M_1

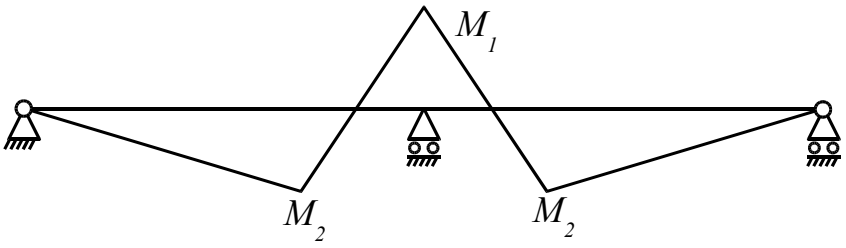

Fig. 12. Collapse bending moment diagram

(5) Formulate the expression balancing external work done by the applied loads F_j acting through virtual displacements δ_j, to that of the internal work done by the hinges $M_i\theta_i$.

$$\sum_j F_j\delta_j = \sum_i M_i\theta_i \qquad 2F\delta = M_1\theta_1 + 2M_2\theta_2 \tag{3.20}$$

Satisfaction of the three conditions of equilibrium, mechanism and cross-section capacity remains a strict requirement in defining the unique plastic collapse load of a structure within the Continuous Strength Method. Thus the collapse bending moment diagram must be in equilibrium with the applied loads and satisfy $M \leq M_{csm}$ at each section throughout, and there should be a suitable number of hinges for collapse. The key diversion from traditional plastic analysis is in the cross-section capacity condition, where the moment capacity M_i may be taken to M_{csm} for each hinge in place of M_{pl}.

It is important to note that, as with traditional plastic design, the method is based on the rigid beam-hinge geometry (which assumes no curvature between the hinges), with all deformation localised at discrete points. This ignores any elastic deformation of the members, and does not include the fact that the material adjacent to the assumed hinge location will have yielded if $M \geq M_{el}$, giving a flexural stiffness between EI and $E_{sh}I$, leading to a hinge zone.

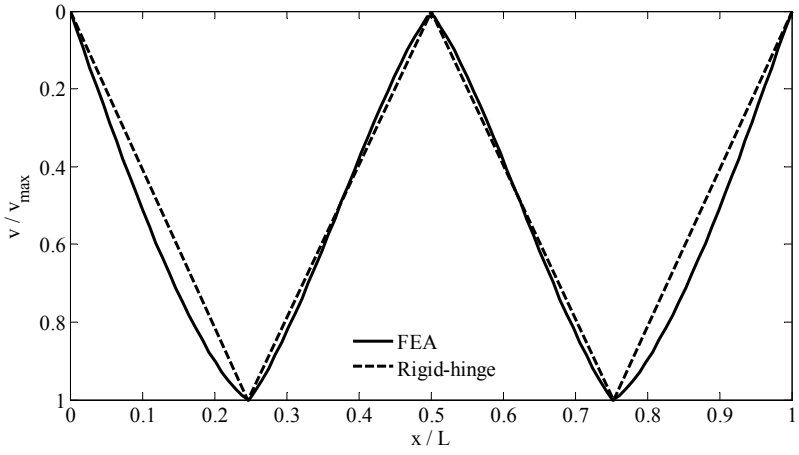

Fig. 13. Assumed plastic collapse vertical displacement and finite element model

This assumed collapse geometry is shown in Fig. 13 against the displacement plot from an ABAQUS finite element analysis (FEA) simulation of beam RHS 60×40×4-HR1, at the ultimate test load F_u using all experimentally recorded geometric and material data. On the vertical axis is v/v_{max}, the vertical displacement normalised by its maximum value and on the horizontal axis, x/L is the normalised position along the length of the continuous beam. The hinge spreading effects as well as the presence of elastic deformations, act to smooth out the beam displacement profile. The collapse shape made up of straight lines between hinges, proves to be a reasonable assumption. The applied load–end rotation plot is shown in Fig. 14 alongside the test measurements and traditional plastic analysis approach. The FEA curve, which includes the CSM material model, shows an improved conformity to the test data at an increased load carrying capacity over traditional plastic design. The complete plastic response of an indeterminate structure can be solved by computer analysis software that can incorporate the CSM strain hardening effects into the model, most easily accounted for by inclusion of the bi-linear material model as highlighted in Fig. 5.

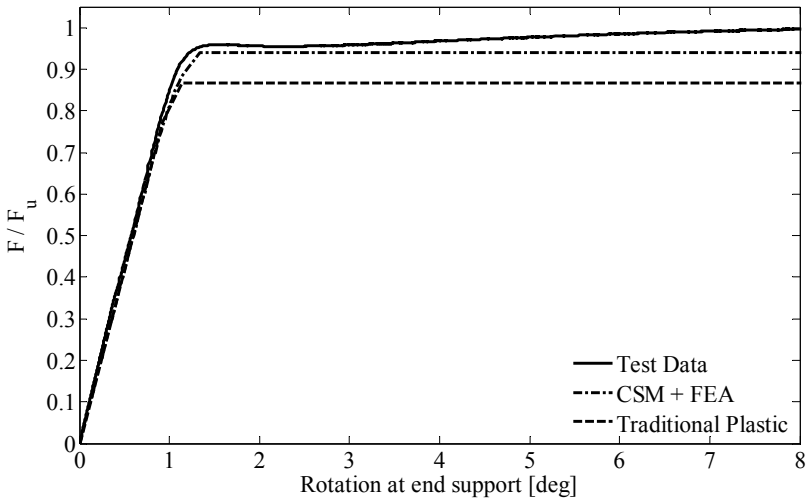

Fig. 14. Load-rotation plot for RHS 60×40×4-HR1

The maximum capacity is reached when $\varepsilon=\varepsilon_{csm}$ (and consequently $f=f_{csm}$ and $M=M_{csm}$) anywhere along the beam. Note that the maximum load obtained from this approach may be marginally different to the collapse load obtained from Eq. (3.20) due to the difference between the assumed and actual geometries as highlighted in Fig. 13; for RHS 60×40×4-HR1 this difference was 1.5%.

3.3.3. Comparison of continuous beam test results with design models

A total of 12 two-span continuous beam tests on steel SHS and RHS were conducted as part of the present study; two configurations were considered; in configuration 1, the loads were applied centrally between the supports (i.e. $L_1=L_2$ in Fig. 11), while in

configuration 2, loads were applied closer to the central support such that $L_1=2L_2$. Comparisons of the results of the continuous beam tests with those obtained from traditional plastic analysis and the CSM are shown in Table 6.

Table 6. Comparison of continuous beam test results with design methods

No. of tests: 12	F_{EC3} / F_u	F_{csm} / F_u	F_{csm} / F_{EC3}
Mean	0. 799	0. 882	1.10
COV	0.078	0.077	-

On average, for configuration 1, $M_1=M_2=1.11M_{pl}$ whereas for configuration 2 the average M_2 is reduced to $1.08M_{pl}$. The Continuous Strength Method may be seen to provide a more accurate prediction of the test behaviour, with an average increase in capacity of 10% over traditional plastic methods.

3.3.4. Comparison of a portal frame test result with design models

Experimental results on full scale steel portal frames are relatively scarce, though one such test has been reported by Ref. 17. The pitched portal frame was constructed from I sections with following properties: f_y=272 N/mm^2, M_{el}=23.2 kNm and M_{pl}=27.4 kNm. The collapse load of the frame was predicted using traditional plastic analysis and the Continuous Strength Method. The collapse loads, as given in Table 7, indicate that the CSM provides a more accurate prediction of the test response, with a 9% increase in capacity over traditional plastic analysis. Further validation of the Continuous Strength Method, based on numerically generated structural performance data is underway.

Table 7. Comparison of portal frame test with design methods

No. of tests: 1	F_{EC3} / F_u	F_{csm} / F_u	F_{csm} / F_{EC3}
	0. 860	0. 940	1.09

4. Conclusions

The importance of strain hardening in the response of determinate and indeterminate steel structures has been highlighted in this paper. It was shown both through experimentation and the analysis of existing test data, that the limiting resistances adopted in present design practice of the yield load in compression for stub columns, the plastic moment capacity in bending for determinate structures and the plastic collapse load for indeterminate structures are conservative in the case of stocky sections, due to the influence of strain hardening. Refinements and developments to the Continuous Strength Method, which offers a rational means of exploiting strain hardening in steel design, have been presented. Extension of the method to cover indeterminate structures, following the principles of traditional plastic analysis but allowing bending moments in excess of the plastic moment capacity, has also been proposed. Comparisons have been made against test results on stub columns, simple beams, continuous beams and a portal frame. These

comparisons show that the CSM provides a more accurate prediction of test response and enhanced structural capacity over current design methods.

Acknowledgments

The authors would like to thank Gordon Herbert, Marios Theofanous and Nadiah Saari for providing assistance during the experimental investigations.

References

1. L. Gardner, *The continuous strength method*. Proceedings of the Institution of Civil Engineers-Structures and Buildings. 161(3) (2008) 127-133.

2. L. Gardner, N. Saari and F. Wang, *Comparative experimental study of hot-rolled and cold-formed structural steel hollow sections*. Thin-Walled Structures. 48 (2010) 495-507.

3. EN 1993-1-5. *Eurocode 3: Design of steel structures – Part 1-5: Plated structural elements*, European Standard, CEN, (2006).

4. B.W. Schafer, Review: *The Direct Strength Method of cold-formed steel member design*. Journal of Constructional Steel Research. 64(7-8) (2008) 766-778.

5. K. J. R. Rasmussen and G. J. Hancock, *Plate Slenderness Limits for High-Strength Steel Sections.* Journal of Constructional Steel Research. 23(1-3) (1992) 73-96.

6. H. Akiyama, H. Kuwamura, S. Yamada and J.-C. Chiu, *Influences of manufacturing processes on the ultimate behaviour of box-section members*. Proceedings of the Third Pacific Structural Steel Conference (PSSC). (1996). Tokyo, Japan.

7. T. Wilkinson and G. J. Hancock, *Tests for the compact web slenderness of coldformed rectangular hollow sections*. Research Report No. R744. University of Sydney, (1997).

8. L. Gao, H. Sun, F. Jin and H. Fan, *Load-carrying capacity of high-strength steel box sections I: Stub columns*. Journal of Constructional Steel Research. 65(4) (2009) 918-924.

9. X. L. Zhao and G. J. Hancock, *Tests to determine plate slenderness limits for cold-formed rectangular hollow sections of grade C450*, Journal of the Australian Steel Institute. 25(4) (1991) 2-16.

10. S. D. Hu, B. Ye and L. X. Li, *Material properties of thick-wall cold-rolled welded tube with a rectangular or square hollow section*, Construction and Building Materials. 25 (2011) 2683-2689.

11. EN 1993-1-1. *Eurocode 3: Design of steel structures – Part 1-1: General rules and rules for buildings*, European Standard, CEN, (2005).

12. M. Seif and B. W. Schafer. *Local buckling of structural steel shapes*. Journal of Constructional Steel Research. 66 (2010) 1232-1247.

13. A. R. Kemp, M. P. Byfield and D. A. Nethercot, *Effect of strain hardening on flexural properties of steel beams*. The Structural Engineer. 80(8) (2002) 188-197.

14. T. Wilkinson and G. J. Hancock, *Tests to examine compact web slenderness of coldformed RHS.* Journal of Structural Engineering-ASCE. 124(10) (1998) 1166-1174.

15. M. P. Byfield and D. A. Nethercot, *An analysis of the true bending strength of steel beams.* Proceedings of the Institution of Civil Engineers-Structures and Buildings. 128(2) (1998) 188-197.

16. J. M. Davies, *Strain hardening, local buckling and lateral-torsional buckling in plastic hinges.* Journal of Constructional Steel Research. 62(1-2) (2006) 27-34.

17. T. M. Charlton, *A test on a pitched roof portal structure with short stanchions.* British Welding Journal. 7 (1960) 679-685.